THE JOURNAL OF PHYSICAL CHEMISTRY B
A JOURNAL OF THE AMERICAN CHEMICAL SOCIETY

pubs.acs.org/JPCB

Article

Conformational Flexibility Is a Key Determinant for the Lytic Activity of the Pore-Forming Protein, Cytolysin A

Avijeet Kulshrestha, Satyaghosh Maurya, Twinkle Gupta, Rahul Roy,* Sudeep N Punnathanam, and K. Ganapathy Ayappa*

Cite This: *J. Phys. Chem. B* 2023, 127, 69−84

Read Online

ACCESS | Metrics & More | Article Recommendations | Supporting Information

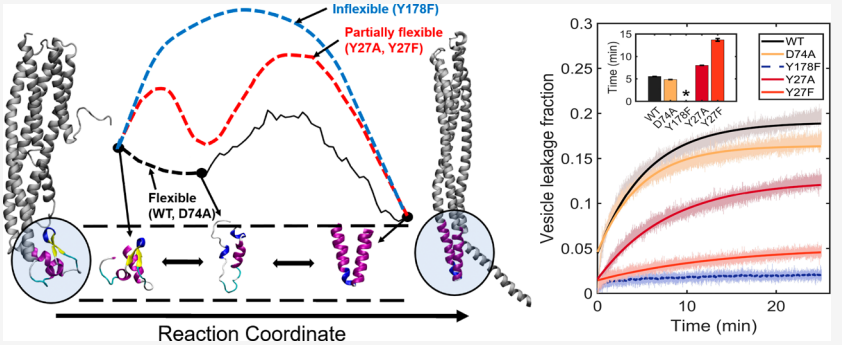

ABSTRACT: Several bacterial infections are mediated by pore-forming toxins (PFTs), a subclass of proteins that oligomerize on mammalian cell membranes forming lytic nanopores. Cytolysin A (ClyA), an α-PFT, undergoes a dramatic conformational change restructuring its two membrane-binding motifs (the β-tongue and the N-terminus helix), during pore formation. A complete molecular picture for this key transition and the driving force behind the secondary structure change upon membrane binding remain elusive. Using all-atom molecular dynamics (MD) simulations of the ClyA monomer and string method based free energy computations with path collective variables, we illustrate that an unfolded β-tongue motif is an on-pathway intermediate during the transition to the helix-turn-helix motif of the protomer. An aggregate of 28 μs of all-atom thermal unfolding MD simulations of wild-type ClyA and its single point mutants reveal that the membrane-binding motifs of the ClyA protein display high structural flexibility in water. However, point mutations in these motifs lead to a distinct reduction in the flexibility, especially in the β-tongue, thereby stabilizing the pretransition secondary structure. Resistance to unfolding was further corroborated by MD simulations of the β-tongue mutant motif in the membrane. Combined with the thermal unfolding simulations, we posit that the β-tongue as well as N-terminal mutants that lower the tendency to unfold and disorder the β-tongue are detrimental to pore formation by ClyA and its lytic activity. Erythrocyte turbidity and vesicle leakage assays indeed reveal a loss of activity for the β-tongue mutant, and delayed kinetics for the N-terminus mutants. On the other hand, a point mutation in the extracellular domain that did not abrogate lytic activity displayed similar unfolding characteristics as the wild type. Thus, attenuation of conformational flexibility in membrane-binding motifs correlates with reduced lytic and leakage activity. Combined with secondary structure changes observed in the membrane bound states, our study shows that the tendency to unfold in the β-tongue region is a critical step in the conformational transition and bistability of the ClyA protein and mutants that disrupt this tendency reduced pore formation. Overall, our finding suggests that inherent flexibility in the protein could play a wider and hitherto unrecognized role in membrane-mediated conformational transitions of PFTs and other membrane protein transformations.

INTRODUCTION

Pore-forming proteins (PFPs) are a special class of proteins expressed as water-soluble monomers by a wide variety of living organisms that can compromise the permeability of cell membranes by self-assembling into transmembrane oligomeric nanopores.[1] Pore-forming toxins (PFTs) represent a large subset of pathogenic PFPs, produced by virulent bacteria to mediate and transmit infections. PFTs are broadly classified based on the secondary structure of the membrane-inserted segments in the pore as α-PFTs (where the pore is lined by a bundle of α-helices) and β-PFTs (where the pore is formed by β-barrels).[2] Cytolysin A (ClyA; also known as hemolysin E (HlyE)), is one of the best studied member of α-pore-forming

Received: August 12, 2022
Revised: October 29, 2022
Published: December 21, 2022

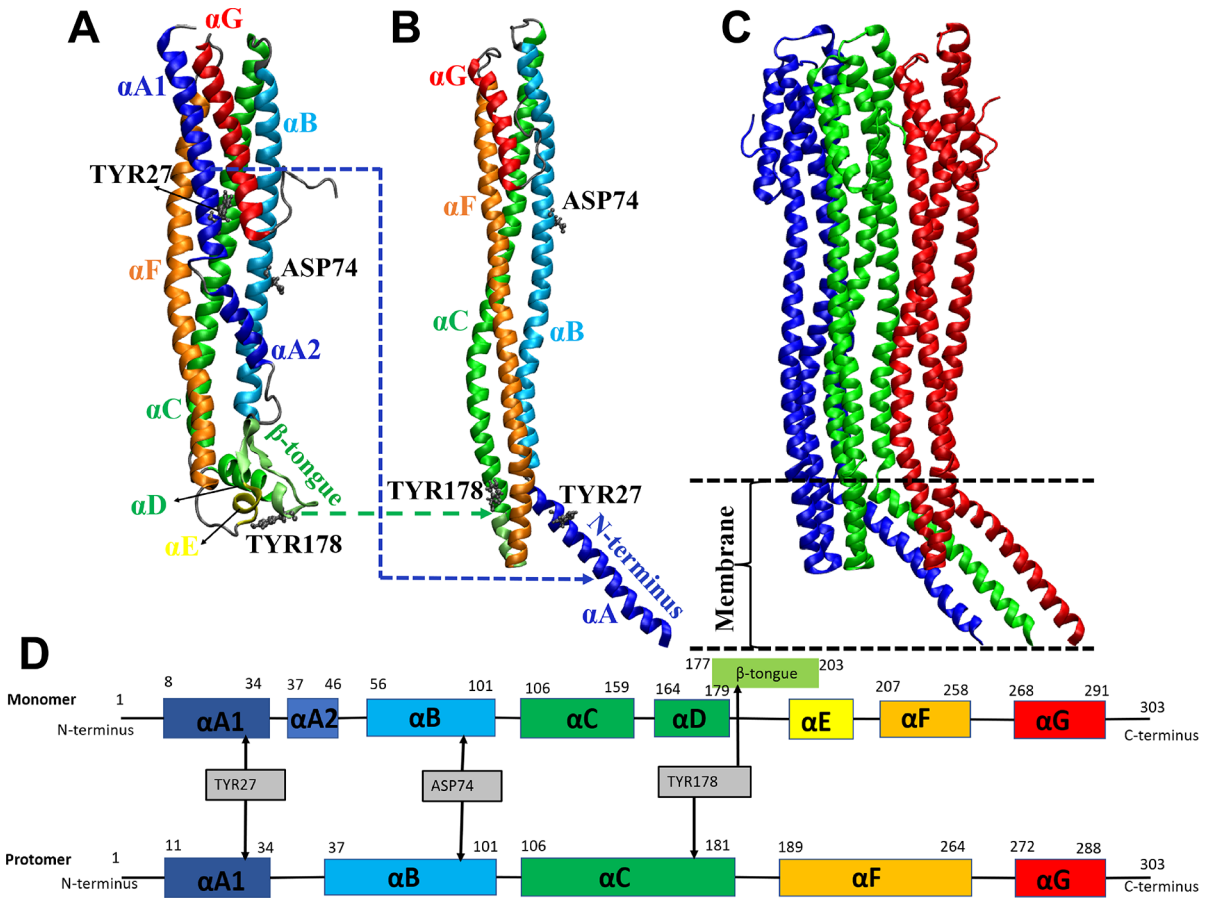

Figure 1. ClyA structure, motifs and position of different point mutations. (A) Monomer structure (PDB ID 1QOY) depicting the β-tongue and the N-terminus that undergo the major conformational changes upon conversion to the membrane-inserted protomer (PDB ID 2WCD) shown in part B. (C) Trimeric protomer system considered in the protomer simulations where the central protomer (green) experiences a full pore like environment. (D) Secondary structure motifs of the monomer and protomer and the location of the different point mutations considered in this study. The color code is similar to that used in parts A and B.

toxin family produced by *Escherichia coli*, *Salmonella typhi*, and *Shigella flexneri*.[1] Remarkably, ClyA is known to undergo one of the largest conformation transitions in the PFT family of proteins, during its conversion from the water soluble monomer form (Figure 1A) to the membrane-inserted protomer state (Figure 1B) as observed in the final dodecameric pore structure.[3] Two membrane-binding motifs of ClyA play a critical role in driving this transition as highlighted by major alterations in their structure and their relative position in the protein between the two states. The highly hydrophobic "β-tongue" (β-hairpin) motif rearranges into a helix-turn-helix motif in its membrane-embedded form. On the other hand, the N-terminus helix detaches from the core helical bundle with a $\sim$ 126° outward movement to reposition itself and form the membrane-inserted hydrophilic transmembrane water channel.[4]

ClyA pore formation is perceived to be initiated by membrane binding with the hydrophobic β-tongue and its subsequent conversion to the helix-turn-helix motif in the membrane[3] (Figure 1A and 1B). Structure based molecular dynamics (MD) simulations[5] support this pathway with membrane interactions dominated by the binding of the β-tongue followed by insertion of the N-terminus to form the membrane-inserted protomeric state (Figure 1B). However, a second minor pathway also showed that the N-terminus can sample the membrane first. Regardless of the initial binding motif, a common intermediate state where both the β-tongue and N-terminus were inserted in the membrane prior to conversion to the protomer was observed. However, the atomic level detail of the intermediate was missing due to the highly coarse grained model structure. In both cases, the predominantly hydrophobic β-tongue must finally undergo a transition to a helix-turn-helix motif in the membrane. The membrane-induced intermediate states sampled during this transition is an open and outstanding question for membrane-induced pore formation. In general, this is important for our understanding from the perspective of how a water-soluble protein can morph into a membrane protein and how the membrane environment can promote the associated structural transitions. Preliminary all atom MD simulations from our group[6] showed that the β-tongue loses its secondary structure when bought in contact with a phospholipid bilayer. However, it has been unclear whether such membrane-induced loss of secondary structure and emergence of a disordered state was a critical intermediate during the transition to the active pore state of the protein.

An intriguing aspect of membrane driven pore formation with PFTs is the influence of specific residues in modulating pore formation. Although one can reconcile loss of activity with truncation mutants,[7] point mutants that can result in a complete loss of activity as observed in ClyA[8] are more complex to understand without atomistic level insights. The

https://doi.org/10.1021/acs.jpcb.2c05785
J. Phys. Chem. B 2023, 127, 69−84

challenge lies in not only obtaining the free energy landscape associated with the conformational change for the large (34 kDa) ClyA protein and variations induced by the point mutations but also obtaining the ability to connect these changes to pore forming activity as observed in bulk vesicle and erythrocyte lysis experiments. In this work, we address this challenge by combining thermal unfolding MD simulations, free energy landscape calculations, membrane-protein MD simulations and vesicle and RBC rupture assays. We propose that the membrane-inserted β-tongue motif of ClyA undergoes a transition through an unstructured intermediate, associated with a loss of secondary structure, to complete the conformation to the pore state. We further demonstrate that point mutants that disrupt this flexibility will in general result in reduced lytic activity.

We first test the hypothesis of an unstructured transition intermediate by examining the conformational change in wild type ClyA. All-atom MD simulations of the monomer embedded in the membrane reveal that the β-tongue indeed starts to unfold while inserted in the membrane. Similarly, simulations with the core β-tongue motif from the monomer also display unfolding and loss of secondary structure when placed in the membrane. We quantified the free energy of transition from a membrane-inserted β-tongue motif of the monomer to the helix-turn-helix motif of the pore state by applying a recently developed string method variant using path collective variables[9] combined with umbrella sampling[10] simulations to evaluate the free energy. The string method originally developed by Weinan et al.,[11] and its variants[12,13] have been widely used to obtain the minimum free energy paths in the collective variables space associated with protein transformations. Using two path collective variables in conjunction with umbrella sampling, we illustrated the utility of the string method by obtaining the free energy landscape of a mini G-protein unfolding from an α-helix to a β sheet.[10] Here, we extend the method, to our knowledge for the first time, to study secondary structure changes in membrane-embedded proteins. The free energy computations illustrate that the membrane-inserted β-tongue motif of the ClyA protein spontaneously unfolds and the simulations captured the free energy landscape during the transition from this unfolded intermediate to the folded motif of the pore state.

As a complementary approach to examine β-tongue flexibility, we resort to thermal unfolding MD simulations of the monomeric form of ClyA in solution. We argue that a greater tendency for the β-tongue to unfold at elevated temperatures would suggest structural flexibility, correlating with a higher propensity to undergo secondary structure transitions at room temperature in the membrane. This would then enable us to study the influence of mutations using thermal unfolding simulations at higher temperatures on the complete ClyA monomer in solvent. *In silico* thermal unfolding of proteins has provided new insights into the underlying mechanism of protein conformational transitions.[14] For example, a point mutation (A21G) in the $A\beta$ dimer (implicated in Alzheimer's disease) that increases the flexibility of the central hydrophobic cluster at 400 K could explain the reduced formation of higher order aggregates.[15] Walser et al.[16] have shown that beyond 400 K protein folding and unfolding pathways are likely to be irreversible. Dinner and Karplus[17] suggest that the unfolding pathway at high temperature and the folding pathways at low temperature are reversible albeit the protein unfolds through many intermediates at lower temperatures. Similarly, Klimov and Thirumalai[18] showed that the folding pathway at 300 K is similar to the dominant unfolding pathway under mild denaturing conditions (390−420 K) using structure-based models. Therefore, initial intermediates in the vicinity of the native state of the protein in thermal unfolding pathways can provide insight into the cooperative motion of protein during folding and unfolding.[19]

In this study, four point mutations at residues of significance are analyzed; one β-tongue mutation−tyrosine 178 to phenylalanine (Y178F), two N-terminus mutations—tyrosine 27 to alanine (Y27A) and phenylalanine (Y27F), and a aspartic acid 74 to alanine (D74A) mutation located in the extracellular region of the pore complex (Figure 1). The motivation for selecting these mutations were based on observations derived from earlier studies where these motifs or residues are implicated in the pore forming pathway of ClyA. The β-tongue residue, Y178, which is solvent exposed in the monomer, is part of the membrane anchoring the RKY (arginine, lysine, tyrosine) motif that forms strong hydrogen bonds with the lipids.[20] Additionally, Y178 provides stacking interactions that favor cholesterol binding to stabilize the pore complex in pockets formed between adjacent β-tongues.[8] Tyrosine 27 (Y27) is part of a cholesterol recognition and consensus motif (CRAC) motif[21] identified on the N-terminus helix[8] that forms the main transmembrane pore channel. Earlier MD simulations and lifetime analysis of salt-bridges found that D74 forms a long-lived salt-bridge between two adjacent protomers in the extracellular region.[22] D74 is part of the core-helical bundle and lies distal to the membrane in the final pore structure (Figure 1) thereby serving as a control in both the experiments and simulations. From the thermal unfolding simulations, we analyze the differential unfolding rates and observed a greater unfolding tendency in the β-tongue for the WT and D74 mutants when compared with the Y27 and Y178 mutants that involve the main membrane-bound motifs.

To correlate our observations from free energy computations and thermal unfolding simulations with pore formation and lytic activity, we carry out erythrocyte lysis and vesicle leakage experiments on small unilamellar vesicles. These experiments provide a direct measure of the pore forming activity of the different mutants. A near complete loss of activity for β-tongue mutant (Y178F) and delayed kinetics for the N-terminus mutants (Y27A and Y27F) are observed. Reduced lytic activity was found to correlate well with the decrease in flexibility of the β-tongue in the thermal unfolding MD simulations. We also carried out MD simulations of a single trimeric arc-like state (Figure 1C) in an attempt to differentiate between the different mutants. However, we did not pursue an extended evaluation of membrane-inserted states[23] since in situations where pore formation is abrogated (Y178F) or reduced, simulating pore states derived from the crystal structure would be unrealistic.

Overall, our study demonstrates that conformational flexibility is indispensable for effective ClyA pore formation and reinforces the central role played by the β-tongue and N-terminal motifs in the ClyA pore formation pathway. Our free energy computations of the membrane-inserted β-tongue motif, combined with thermal unfolding simulations of the full monomer, provide compelling evidence to suggest that the transition to a helix-turn-helix motif of the ClyA oligomeric pore state proceeds via a key disordered β-tongue intermediate that follows membrane binding. Mutations that disrupt this

https://doi.org/10.1021/acs.jpcb.2c05785
J. Phys. Chem. B 2023, 127, 69−84

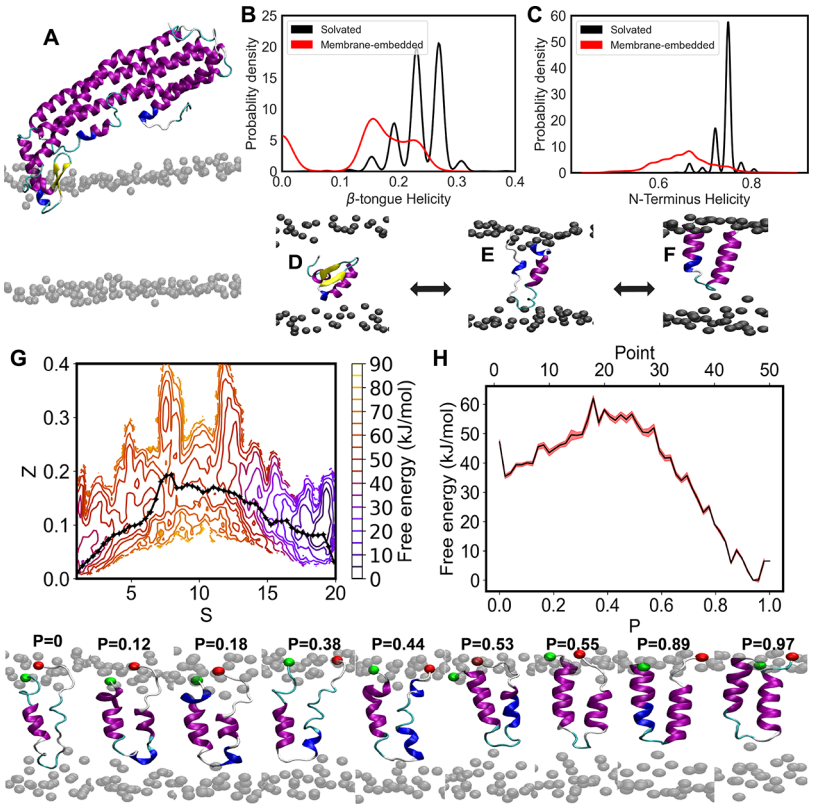

Figure 2. Conformational transitions of monomer β-tongue embedded in the membrane. (A) Final configuration of the ClyA monomer inserted in the membrane at the end of 1 μs. The comparison of the change in the helical content between the solvated and membrane-embedded protein for the β-tongue (B) and N-terminus (C), respectively. (D) Initial configuration of the truncated β-tongue in the membrane where only lipids head groups are shown for clarity. (E) Final disordered state of the truncated WT β-tongue. (F) Truncated protomer state of the WT considered in the simulation. (G) 2D free energy contour plot for the transition from unfolded state illustrated in part E, at S = 1 to protomer state illustrated in part F, at S = 20. The black line illustrates the location of the transition path consisting of 50 points. (H) 1D free energy profile along the transition path as a function of the parametrized distance "P". Below are the snapshots of the states on the transition path, where the N-terminus of the protein is shown with a green sphere and the C-terminus is shown with a red sphere.

tendency to unfold resulted in reduced attainment of the promoter state, and erythrocyte lysis and vesicle leakage experiments support this view.

MATERIALS AND METHODS

Cytolysin A Monomer Simulation Details. Crystal structure of ClyA monomer (PDB ID 1QOY)[24] was used as an initial structure where the missing residues (299−303) were modeled using Modeler 9.9 as a loop while keeping the remaining atoms fixed (see Figure 1A). VMD software[25] was used to perform four point mutations (Y178F, Y27A, Y27F, and D74A) in the monomer. The monomer was solvated with TIP3P water and Na^+ and Cl^- ions were added to yield a 150 mM of salt concentration. Initial structures were energy minimized, followed by equilibration of 2 ns in the *NVT* ensemble and 10 ns in the *NPT* ensemble with position restraints. Ramachandran plots of final equilibrated structures of monomer are given in Figure S2. The final configurations from the equilibration simulations were used as the starting structures for the production runs. All monomer simulations were performed in the *NPT* ensemble using GROMACS-2018.6 with the force field parameters for the ClyA protein taken from CHARMM36.[26] Using the X-ray crystal structure data of ClyA, we have previously modeled[23] the entire dodecameric pore complex of ClyA using CHARMM36 and found excellent agreement with the pore dimensions reported in the crystal structure.[3] The CHARMM36 force field has also been used to study the unfolding and refolding mechanism of ClyA in free solvent.[27] Equilibration was monitored by evaluating the root mean squared deviations (RMSD) for the protein. Simulation of the wild type and all mutants were performed at three different temperatures: 310, 350, and 400 K. Details of the monomer simulations are given in Supporting Information (see Table S1). Based on previous studies,[16−18] the highest temperature of 400 K was used to analyze differential unfolding and conformational changes between the proteins. For improved statistics, three independent 1 μs long simulations were performed at 400 K for all the different systems and properties averaged across these three simulations sets are reported. Unless stated otherwise, all the data presented at 400 K represent averages over the three independent simulations. At 300 and 350 K, we did not observe any tendency of the proteins to disorder, and single simulations were carried out for 350 ns during which the systems appear to have equilibrated. These simulations were carried out primarily to infer the temperature at which thermal denaturing would occur.

Membrane-Embedded Cytolysin A Simulation Details. Microsecond long all-atom MD simulations for the membrane-inserted trimer arc protomer state of ClyA (both the wild type and mutants) were performed on a POPC:cholesterol (70:30) membrane. The initial structure

https://doi.org/10.1021/acs.jpcb.2c05785
J. Phys. Chem. B 2023, 127, 69−84

of the bilayer was generated using the CHARMM-GUI membrane builder.[28] For each membrane-inserted complex, we considered three successive ClyA proteins (3-mer, Figure 1C) from the dodecameric transmembrane pore crystal structure (PDB ID 2WCD)[3] by eliminating the rest of the protomers. Unresolved residues of N-terminal (1 to 7), and C-terminal (293 to 303) were modeled using Modeler 9.9.[29] Complete details of membrane-inserted trimer arc simulations is given in the Supporting Information (see Table S2). Similar protocols as the monomer were used for initialization of the membrane-inserted structures. All protomer simulations were performed in the *NPT* ensemble at 310 K using GROMACS-2018.6 with the force field parameters for the ClyA protein taken from AMBER99SB, and the force field parameters for lipid and cholesterol taken from the SLIPIDS force fields.[30−32] MD simulations of ClyA oligomers using similar force fields have shown promising results in our laboratory.[8,23,33,34]

All-atom simulations of the monomer with its β-tongue embedded in POPC:cholesterol (70:30) membrane (Figure 2A) and three replicates of 500 ns long for the truncated β-tongue (residues 170−207) in the membrane (Figure 2D) were performed with the same protocols as trimeric protomer simulations. The β-tongue was truncated based on the previously found membrane−residue interaction in the protomer state[23] and positioned at the center of the membrane in the initial configuration. The simulation details of the monomer in the membrane at 310 K are given in Table S3.

Free Energy Computations Using the String Method. We use the method developed in our recent work,[10] where we studied the transition of the mini G-protein. Here, we extend the method to study conformation transitions of the β-tongue motif of ClyA embedded in a POPC:cholesterol (70:30) membrane. Two stable end points of the string were carefully selected based on multiple replicates of equilibrium simulations of membrane-inserted monomer and protomer states. The conformational space was defined using path collective variables (PCVs) originally developed by Branduardi et al.[9] Let the protein consist of N particles with positions $(\mathbf{r}_1, \mathbf{r}_2, ..., \mathbf{r}_N) \equiv \mathbf{R}$. The path is constructed by defining a sequence of M membrane-inserted reference structures, $\{\mathbf{R}^{(1)}, \mathbf{R}^{(2)}, ..., \mathbf{R}^{(M)}\}$ between the unfolded β-tongue motif and the helix-turn-helix motif which form the two end states of the protein for which the free energy path is computed. The two path collective variables are

$$S(\mathbf{R}) = \frac{\sum_{j=1}^{M} j e^{-\lambda D(\mathbf{R}^{(j)},\mathbf{R})}}{\sum_{j=1}^{M} e^{-\lambda D(\mathbf{R}^{(j)},\mathbf{R})}}$$

and

$$Z(\mathbf{R}) = -\frac{1}{\lambda} \ln\left(\sum_{j=1}^{M} e^{-\lambda D(\mathbf{R}^{(j)},\mathbf{R})}\right) \quad (1)$$

where

$$D(\mathbf{R}^{(j)}, \mathbf{R}) = \frac{1}{N}\sum_{i=1}^{N} |\mathbf{r}_i^{(j)} - \mathbf{r}_i|^2 \quad (2)$$

is the mean square distance between the jth reference state and dynamic coordinates of the protein during the evolution of the path. S and Z provide a measure of the distance along and perpendicular to the path, respectively.[9] The reference path that is needed to define the PCVs, consisted of 20 states, generated using the Gromacs morph feature which linearly interpolates between the two end states. The λ values were used as (594.88 nm^{-2}), which is inversely proportional to the mean square displacement (MSD) between two consecutive states on the reference path.

The string was defined by 50 points connecting the initial and the final state. The method for evolution of the string is based on umbrella sampling simulations, where each window is a point on the string. The biasing potential is a function of the collective variables S and Z, and it is defined using the harmonic forms

$$\Psi(S, Z) = \frac{k_s}{2}[S(\mathbf{R}) - S_0]^2 + \frac{k_z}{2}[Z(\mathbf{R}) - Z_0]^2 \quad (3)$$

where S_0 and Z_0 are the location of the images on the string. Their values are determined using the average values of S and Z from the previous iteration. This is followed by a reparameterization step to obtain equidistant images along the string.[11] The force constants k_z and k_s are 100 kJ/mol. During string evolution, 0.5 ns of simulations were performed on each point in every iteration until the string converged. Convergence of the string is monitored using the function

$$C = \frac{1}{P}\sum_{j=1}^{P} \|\boldsymbol{\theta}_j^{(k+1)} - \boldsymbol{\theta}_j^{(k)}\| \quad (4)$$

where θ_j represents the coordinates (S_j, Z_j) and $\|\cdot\|$ is the Euclidian norm. The superscript k is the iteration number and subscript j represents the point on the string. The convergence of the string was achieved in 11 iterations (Figure S1E). Additional 50 ns umbrella sampling simulations on each point of the converged string were performed to obtain sufficient overlap of the histograms. We ensured sufficient overlap of the 2D histograms, which is a necessary condition for the WHAM analysis, by examining regions with sampling counts greater than 0.1 million as illustrated in Figure S1F. The 1D free energy profile was reported on the arc length parametrized distance "P" calculated from the monomer state to the protomer state. In order to check the convergence of the free energy profile, we performed the WHAM analysis at successive addition of 5 ns of simulation (Figure S1G). The results are illustrated in Figure S1G, which indicates that the free energy is invariant beyond 40 ns with negligible change observed between 45 and 50 ns of simulations.

Simulation Analysis. Trajectory analysis was carried out using in built GROMACS commands and MDAnalysis python tool.[35] Time trajectories of secondary structure changes were monitered using Gromacs do-dssp command and VMD timeline features with the STRIDE software.[25,36,37] Tilt angles were calculated between a vector normal to the membrane and a vector connecting the first and last residue of the N-terminus. The variation in the distance, r, between the residues in the monomer was modeled by a harmonic oscillator to evaluate the spring constant[23] from the probability distributions of the distance. Carrying out ensemble averages in the canonical ensemble for a harmonic oscillator with a spring constant, k, one obtains

$$k = \frac{k_B T}{\langle r^2\rangle - \langle r\rangle^2} \quad (5)$$

https://doi.org/10.1021/acs.jpcb.2c05785
J. Phys. Chem. B 2023, 127, 69−84

where k_B is the Boltzmann constant, T is the temperature, and $\langle r^2\rangle - \langle r\rangle^2$ is the variance in the distance, r between the two residues. Residue-wise change in the local secondary structure was evaluated using the deviation for a given secondary structure, i from the corresponding structure in the crystal state. We evaluate this using

$$\Delta P_i = P_{i,\text{simulation}} - P_{i,\text{crystal structure}} \quad (6)$$

where, $P_{i,\text{simulation}}$ is the fraction of time spent by the ith residue in a helical state. $P_{i,\text{crystal structure}}$ is either 0 or 1 for a given residue. Using this definition, ΔP_i varies between −1 to +1. A value of −1 indicates that a residue which was in a helical state has completely lost its helicity, a value of +1 indicates that a nonhelical residue has become helical, and a value of 0 indicates that the secondary structure of the residue has remained unchanged. A similar analysis can be performed for any secondary structure content. We also evaluate the value of ΔP_i between the crystal structures of the monomer and protomer.

EXPERIMENTAL METHODS

Site-Directed Mutagenesis and Protein Purification. Polymerase chain reaction (PCR) for site-directed mutagenesis (SDM) was performed using nonoverlapping mutation primers and pET11a-ClyAQ56C as the template to obtain the ClyA mutants. A mutation at the 56 residue to cysteine did not perturb the lytic activity of ClyA.[8,38] Plasmid amplicons with mutations incorporated were ligated and transformed into *E. coli* DH5α and resulting colonies were verified by sequencing. *E. coli* BL21(DE3) cells harboring the ClyA plasmid(s) were induced with 500 μM IPTG at 25 °C overnight. The protein was purified by Ni-NTA affinity chromatography and dialysis as previously described.[8]

Red Blood Cell Turbidity and Liposome Dye Leakage Assay. Kinetic measurements of human erythyrocyte lysis (1%, v/v in PBS) by all ClyA mutants (at 10 μM) were performed using a plate reader (Thermo Fisher, Varioskan reader) at 37 °C in shaking mode (120 rpm). The lysis curve (C_{lysis} versus time, t) was fitted using a Boltzmann sigmoidal function

$$C_{lys}(t) = C_{R,\text{sat}} + (C_0 - C_{R,\text{sat}})(1 + e^{t - t_{lys}/C_{R,\text{slope}}})^{-1} \quad (7)$$

to determine the lysis half-life, t_{lys}. In eq 7, C_0, $C_{R,sat}$, and $C_{R,slope}$ are the starting optical density (OD), the final OD, and the slope of the Boltzmann sigmoidal function, respectively.

Small unilamellar vesicles (SUVs) were preloaded with sulforhodamine B (SRB) (Merck) dye at a self-quenching concentration of 25 mM. Briefly, 1-palmitoyl-2-oleoyl-glycero-3-phosphocholine (POPC) and cholesterol (Avanti Polar Lipids, USA) in 70:30, mol % at 6 mM final concentration was incubated overnight at 37 °C with 25 mM Sulforhodamine B (SRB). SUVs were generated by sonication for 2 h, and excess SRB dye was removed by gel filtration. Increase in fluorescence due to dequenching of the dye upon vesicle rupture by addition of ClyA is measured in a fluorescence spectrophotometer (Agilent Cary Eclipse). The leakage curve (C_{leak} versus time, t) was fitted to an exponential decay function,

$$C_{leak}(t) = C_L e^{-t/t_{leak}} + C_{L,\text{sat}} \quad (8)$$

to determine the leakage time constant (t_{leak}). In eq 8, C_L and $C_{L,sat}$ are the coefficient and saturated intensity levels in the dye leakage curve, respectively.

Binding of ClyA to Erythrocytes. ClyA was labeled with Cy3-maleimide dye at the Cys56 residue as previously described.[8] This labeling does not compromise pore forming activity.[8,38] To quantify the level of binding of ClyA proteins to erythrocytes, 50 nM of labeled ClyA was incubated with RBCs for 5 min. The cell suspension was then centrifuged at 8000 rpm for 2 min and the supernatant was collected and measured using a fluorescence spectrophotometer (Agilent Cary Eclipse). Using a similar measurement without the RBCs, total ClyA added was calculated separately and used to estimate the fraction of ClyA bound to the RBC membrane.

RESULTS AND DISCUSSION

Unfolding of the β-Tongue Initiates the Conformational Change from Monomer to Protomer. Since the pathway for ClyA monomer binding and ensuing conformational changes is perceived to be initiated with the binding of the predominantly nonpolar β-tongue to the lipid membrane,[3,23] we simulated the ClyA monomer with it is β-tongue inserted into the POPC/cholesterol (70:30) membrane at 310 K. The final configuration at the end of the 1 μs simulation is shown in Figure 2A. Upon comparison with the monomer in water, a clear loss of secondary structure is observed in the β-tongue region (Figure 2B). In addition to the β-tongue, we observe the N-terminus starting to lose helical content (Figure 2C) indicating that the conformational change in the ClyA monomer is accompanied by secondary structure changes in both these primary membrane bound motifs and allosteric effects that exist between the inserted β-tongue and the N-terminus of the monomer present in the extracellular helical bundle (Figure 1A). Note that complete pore formation involves insertion of the N-terminus into the membrane to form the transmembrane pore channel (Figure 1B).

To further understand the unfolding of the β-tongue, we simulated a membrane-inserted β-tongue motif comprising of residues 170−207 (Figure 1D). This tendency to spontaneously disorder (to be discussed later in the text) was observed in all three 500 ns long replicates reinforcing the tendency of the β-tongue to lose secondary structure as observed in the fully inserted monomer simulations. In Figure 2E, the final state of the WT β-tongue illustrates an unfolded state with the terminal residues bound to the head groups of the lipid molecules resembling the positioning of the β-tongue in the protomer or pore state. This partially unfolded state was found to be stable over an additional 500 ns of MD simulations (S1B).

The MD simulations of the truncated β-tongue and the fully inserted monomer reinforce the view that β-tongue unfolding occurs spontaneously at room temperature, manifesting the first step in the conformational pathway of ClyA from a water-soluble monomer to the membrane-inserted protomer (Figure 1). In order to assess the barrier to transform from the unfolded intermediate (Figure 2E) to the helix-turn-helix motif of the pore state (Figure 2F), we apply the finite temperature string method on path collective variables to capture the transition between the two stable states, i.e., the partially unfolded state and the helix-turn-helix state. The convergence of the string is given in Figure S1E. A 2D free energy landscape along with the location of the converged string is shown in path collective variable space S and Z (Figure 2G), where the string is defined by 50 points on the path. In Figure 2H, the free energy profile along the string shows the free energy difference between the protomer and the monomer state as

https://doi.org/10.1021/acs.jpcb.2c05785
J. Phys. Chem. B 2023, 127, 69−84

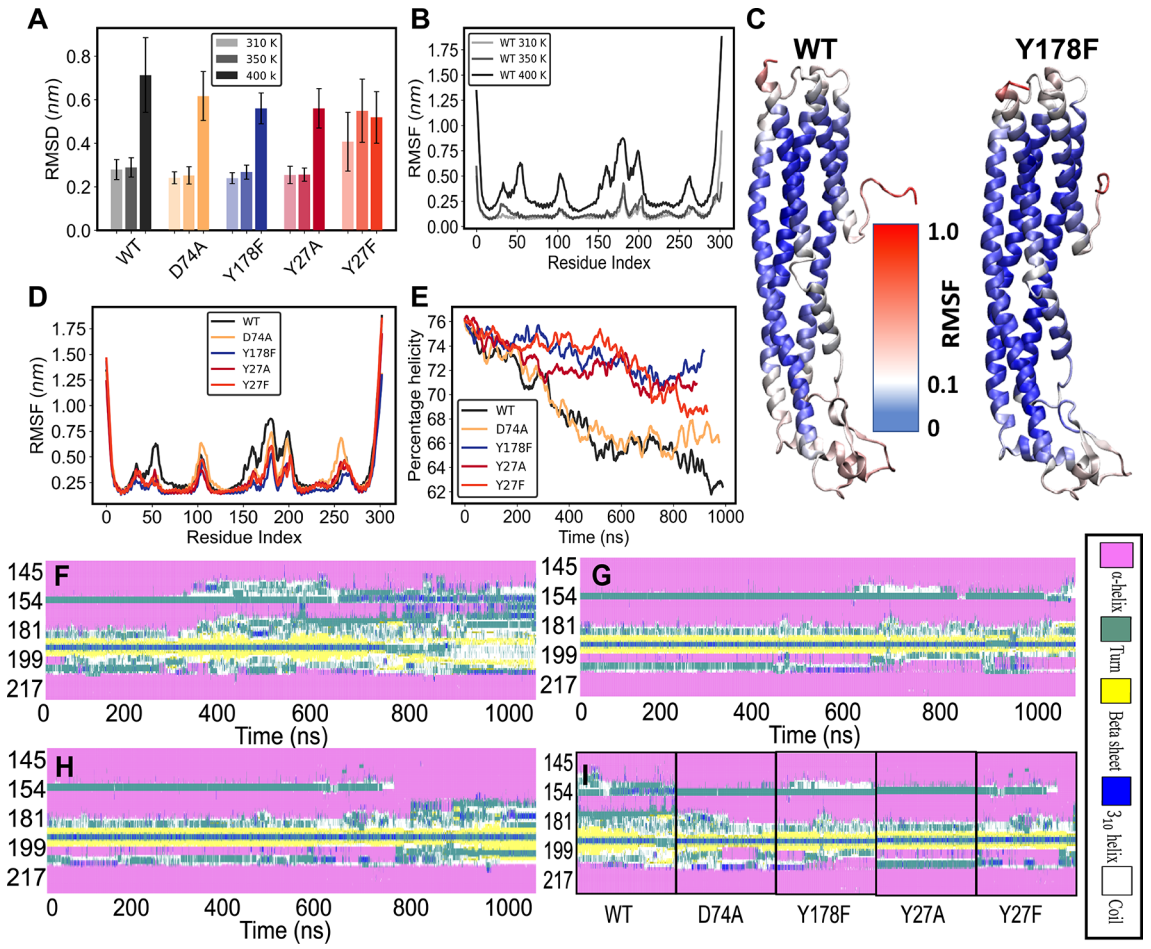

Figure 3. Thermal unfolding analysis of ClyA monomer. (A) Root mean square deviation (RMSD) comparison of the monomer at 310, 350, and 400 K. (B) Root mean square fluctuations (RMSF) of the C_α atoms of WT monomer. (C) Structure of WT and Y178F depicting the normalized RMSF variation as a heat map. (D) RMSF of the C_α atoms of monomer mutants at 400 K. (E) Percentage helicity of the entire ClyA protein at 400 K with time. Secondary structure motif assignments around the β-tongue region from the first set of simulations at 400 K for (F) WT, (G) Y178F, and (H) Y27F as a function of the simulation time. (I) Secondary structure comparisons of the β-tongue region between ≃600 and 800 ns for the different ClyA variants. A similar behavior of secondary structural change was observed in replicates.

−35.43 ± 0.77 kJ/mol, indicating the favored formation of the helix-turn-helix motif of the membrane-inserted protomer state. The transition from the partially unfolded state occurs through an initial barrier of 26.56 ± 1.95 kJ/mol. During this transition (lower panel of Figure 2), we did not observe the refolding to the β-sheet state (Figure S1H). The helicity of the N-terminal strand almost remains intact during the transition; however, the C-terminal side strand initially fluctuates between the coil, α-helix, and 3_{10}-helix. Around p = 0.53, the helix along the C-terminal end begins to form, progressively completing the conversion to the helix-turn-helix motif. Although this might appear to be a large barrier for this refolding transition, we point out that these values are for the isolated β-tongue. The energetics of this transition would be different for the full monomer and influenced by the presence of other proteins during the assembly process.

Observations from the membrane-inserted free energy computations confirm that partial unfolding of the monomer is an essential step for the overall conformational transition during ClyA pore formation. This step is followed by a refolding event to complete the conformational change; however our simulations show that the initial unfolding of the β-tongue motif is critical. We further analyze the unfolding of the solvated WT monomer and it is mutants using thermal unfolding simulations in the next section.

Monomer *In Silico* Thermal Unfolding Reveals β-Tongue Flexibility. To examine the effect of critical mutations on monomeric ClyA, we simulated all-atom models of ClyA variants at elevated temperatures (310, 350, and 400 K) to induce partial unfolding of the protein. We evaluate the root mean squared deviation RMSD over the μs long simulations (Figure S3C). At 400 K, an increase in the RMSD is observed for all of the variants, suggesting the onset of significant unfolding and major secondary structural changes in the ClyA monomer (Figure 3A). Interestingly, RMSD changes are the largest for the WT followed by D74A. When we evaluate the WT root-mean-square fluctuation (RMSF), progressive destabilization of ClyA motifs becomes evident with increase in temperature (Figure 3B). We observe that the N-terminus and C-terminus helices start to destabilize significantly at 400 K. This is consistent with the experimental observation of their unfolding under chemical denaturation by Dingfelder et al.[39] Furthermore, the simulations at 400 K show that helix-turn-helix motifs between αF-αG helices (258−268) and αB-αC helices (101−106) are also destabilized (Figure 3, parts B and C). However, the most significant fluctuations are observed in the neighborhood of the β-tongue motif (150−

https://doi.org/10.1021/acs.jpcb.2c05785
J. Phys. Chem. B 2023, 127, 69−84

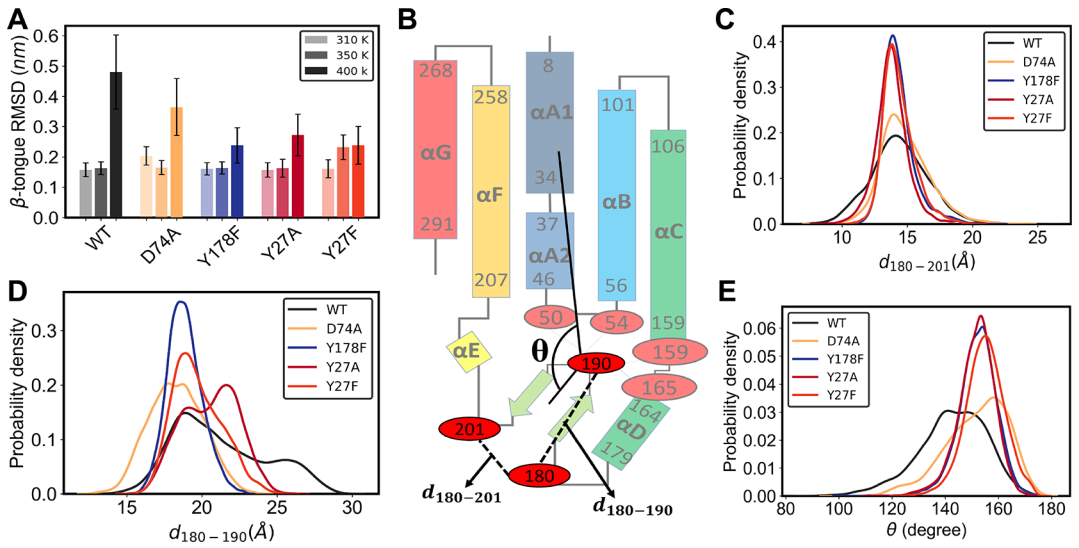

Figure 4. β-tongue flexibility in the ClyA monomer simulations. (A) RMSD comparison of the β-tongue (residues 177−203) at different temperatures. (B) Location of hydrophobic residues (red ovals) that makeup the hinge region of the β-tongue pocket with distances and angles used in the analysis. (C) Probability distribution of distance between residues 180−201, $d_{180-201}$ at 400 K. (D) Probability distribution between residues 180−190, $d_{180-190}$ at 400 K. (E) Angle distribution between a vector from center of mass of the β-tongue to Phe190 and a vector from center of mass of the N-terminus to Phe190 at 400 K as illustrated in part B.

206) and the αA2-αB (46−60) segment that lies in close proximity to the β-tongue in the monomer conformation (Figures 1A). We attribute this to the flexibility of the β-tongue motif that enables its facile opening from the hydrophobic core and rearrangement of its secondary structure in the final pore state. Comparison of the RMSFs at 400 K revealed that the WT has significantly pronounced fluctuations compared to the other mutants, especially in the β-tongue region (Figures 3, parts C and D). With the exception of Y178F whose fluctuations are distinctly lowered (Figure 3D), the other mutants show increased RMSF in the loop regions but the large fluctuations in the surrounding helices evident in the WT were not observed. The reduced fluctuations for the mutants suggest that conformational changes in these critical regions might be compromised. An additional indicator of the global secondary structure changes of ClyA is the temporal evolution of the helical content in the protein. The WT demonstrates the greatest decrease in the overall helicity over the course of the μs long simulation at 400 K (Figure 3E), highlighting the inherently increased structural flexibility of the WT ClyA. D74A mutant shows similar reduction in helicity as the WT; however, the tendency to lose helicity has been compromised in other mutants to different extents. We quantify the rate of helicity loss between the different proteins later in the manuscript.

Since the ClyA structural transition to the protomer form is triggered by the opening of the β-tongue,[3,5] we examined the secondary structure changes in this region illustrated in Figure 3F to Figure 3I. The αD (164−179) helix of the protein in the WT (Figure 3F) progressively loses helicity over the course of the simulation. Simultaneously, the central segment of the β-tongue (177−203) converts into a turn motif, implying that the secondary structure of the native ClyA monomer is susceptible to disruption (Figure 3F and Figure S4). The innate flexibility in the β-tongue is crucial to form the helix-turn-helix motif upon the interaction with the membrane and the secondary structure analysis in this region reveals interesting differences across the various mutants. In contrast to the WT, we did not observe any significant disruption of the secondary structures in Y178F and Y27A mutants (Figures 3G and Figure S4, respectively) suggesting that these mutations impair the flexibility of the β-tongue. The Y27F mutant displays a loss of helicity in the αD motif only beyond 800 ns, at the cost of gaining helicity in the neighboring residues, 160−163, (Figure 3H) which fuses the monomer helices αC and αD into a single helix (αC) in the protomer state. The D74A mutant (Figure S4B) shows increased coil formation in the residues that form part of the αD helix, and the induced secondary structure changes are greater when compared with other mutants, however less than those observed in the WT (Figure 3D). The secondary structure changes between 600 and 800 ns of the simulation (Figure 3I) clearly reveal that the tendency to disorder is greatest in the WT followed by D74A, with the other mutants showing greater resistance to disorder. In order to evaluate a comparison in the secondary structure changes, we next focus on the structure of the β-tongue and evaluate various properties to quantify the extent of flexibility in this region (Figure 4).

To characterize the β-tongue fluctuations, we monitored the RMSD (Figure 4A) and a few critical distances and angles as illustrated in Figure 4B. At 400 K the β-tongue RMSD is higher for the WT and D74A mutant when compared with the other mutants. G180 and G201 residues act as a hinge serving as pivots during the release of the buried β-tongue.[3] Consistent with this mechanism, a G180 V mutant has been found to compromise hemolytic activity[40] of ClyA. Interestingly, the distance distribution between these two residues, $d_{180-201}$ displays the largest spread for the WT and D74A mutant (Figure 4C). Upon modeling the distance distribution $d_{180-201}$ using a harmonic oscillator (eq 5), it is evident that WT and D74A have characteristically lower spring constants compared to the other mutants (Table 1).

Another critical residue in the β-tongue, F190 is located at the tip of the β-tongue forming hydrophobic interactions with the terminal residues of four helices, αA2, αB, αC, and αF, as illustrated in Figure 4B. The distance between G180-F190,

https://doi.org/10.1021/acs.jpcb.2c05785
J. Phys. Chem. B 2023, 127, 69−84

Table 1. Force Constant for the Distance and Angle Variations

protein	$k(d_{180-201})$ (pN nm^{-1})	$k(d_{180-190})$ (pN nm^{-1})	$k(\theta)$ (J mol^{-1} deg^{-2})
WT	111.62	57.43	20.13
D74A	150.62	171.79	24.29
Y178F	349.06	417.43	63.07
Y27A	325.30	160.52	68.08
Y27F	365.43	209.42	62.22

$d_{180-190}$ provides a measure of the extent to which the β-tongue is buried within this hydrophobic pocket. Again, we observe the largest spread in the distance distributions between these residues for the WT, smallest variation for Y178F, with the mutants showing variations that lie between. The spring constant for the distance distribution $d_{180-201}$ clearly shows the lowest value for the WT and highest for Y178F (Table 1). A higher variation is an indication of the larger inter-residue motion and increased flexibility required for effective release of the β-tongue from the hydrophobic core of the ClyA monomer during pore formation. Increased fluctuation in $d_{180-190}$ could facilitate the repositioning of the β-tongue, indirectly influencing the movement of the N-terminus via the interaction of the terminal F50 with residue F190 (Figure 4B). In order to quantify this movement, we calculated the angular distribution θ between the center of mass of the β-tongue and N-terminus with F190 as the vertex (Figure 4B). The θ distribution for the WT ClyA showed the greatest spread dominated by values around 140°, and D74A also showed high variation with a peak around 160°. The other mutants mostly sample conformations where $\theta \sim 155°$ and show limited spread in the distributions (Figure 4E). The spring constant for the angle distribution showed the lowest value for WT followed by D74A, and significantly higher values for the other mutants. A small angle and small spring constant for the WT implies an increased propensity for the N-terminus (αA1) to flip out from the groove formed by the four helices which contains the β-tongue (Figure 1A) during the protomer formation (Figure 1B).

To further quantify the extent of secondary structure changes affected by the mutations, we evaluated the residue-wise average change in the local helicity across the different mutants using eq 6. The loss or gain in the helicity of each residues in the WT and mutant proteins is shown in Figure 5A. In addition, the changes that occur from monomer to protomer are also illustrated in the first row of Figure 5A. The helical content for residues 160−175 (in αD) and residues 192−200 (part of the β-tongue) remain unchanged for all the mutants except for the WT and D74A. The loss of helicity in the WT and D74A occurs predominantly in the vicinity of the loops which convert to the larger helices (αC and α F) upon transformation to the protomer (first row of Figure 5A, Figure 1D). The loss of helicity in the monomer around the helix-turn-helix motif of the β-tongue is correlated with the formation of α-helices upon membrane insertion. Thus, the propensity to undergo a conformational change in the β-tongue region of the ClyA monomer appears to be related to the tendency to lose helicity, and this trend is only observed in the WT and D74A mutant.

The N-terminus (αA1) inserts into the membrane by flipping out from the helical bundle in the monomer (Figure 1A). αA1 is connected to αA2 by a small turn (34−37) which converts into a helix upon membrane insertion. At 400 K, we see a high propensity of helix formation around residue number 30 in the WT and D74A, again indicative of the increased propensity to induce secondary structural changes during the formation of the protomer (Figure 5). Interestingly, all the mutants show a small increase in helicity for residues 176−179 which form part of the terminal end of αD which fuses with the β-tongue to form the extended αC helix (Figure 1). Snapshots of the β-tongue residues in Figure 5B illustrate the increased disorder and loss of helicity for WT and D74A.

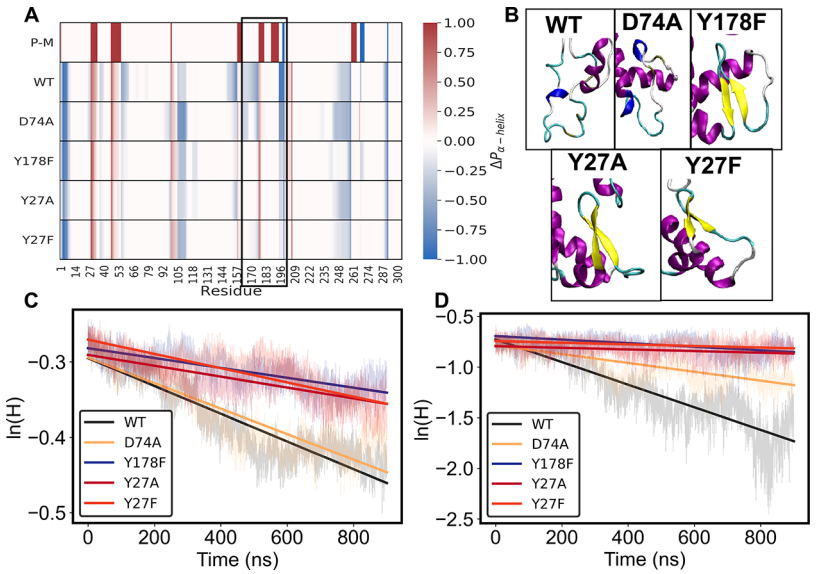

Figure 5. Residue-wise change in α-helicity of monomer mutants. (A) ΔP_i (eq 6) for the α-helix at 400 K. Positive values (red) indicates an increase in helicity and negative values (blue) indicate a decrease in helicity. Rectangular box depicts the β-tongue residues. (B) Snapshots taken at 700 ns from first run at 400 K show a distinct decrease in helicity of the β-tongue regions in WT and D74A. Color coding is similar to Figure 3. (C) Change in helicity, H, with time of the entire protein and (D) for the β-tongue. Solid lines represent the single linear fit to the equation $\ln H(t) = \ln H_0 - \frac{t}{\tau_H}$.

https://doi.org/10.1021/acs.jpcb.2c05785
J. Phys. Chem. B 2023, 127, 69−84

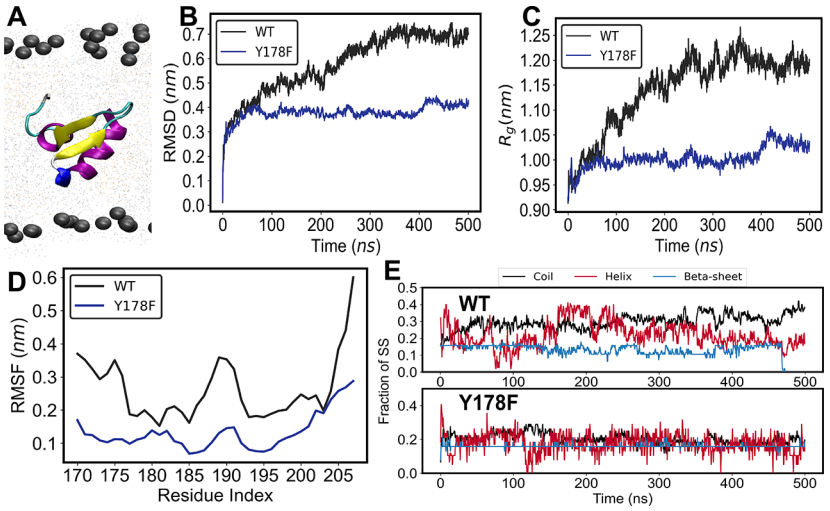

Figure 6. (A) Initial state of the truncated β-tongue in the membrane. The comparison of the average change from three independent simulations in the structural properties of β-tongue in membrane. (B) Root-mean-square deviation (RMSD), (C) radius of gyration (R_g), and (D) root-mean-square fluctuation (RMSF). (E) Comparison of the fraction of the secondary structure change with time between the WT and Y178F truncated β-tongue.

In contrast, the β-sheets are stable for all the mutants and the extent of disorder around this region is substantially reduced. In order to quantify the evolution of helicity over time ($H(t)$), we approximate the loss of helicity of the entire protein and the β-tongue region separately using a first order kinetics model. The temporal change in helicity from the simulations are fitted using $\ln H(t) = \ln H_0 - \frac{t}{\tau_H}$, where H_0 is the initial helicity and τ_H is the corresponding time constant as illustrated in Figure 5, parts C and D. Using this model, the τ_H values for the WT and D74A were 543 and 591 ns, respectively, whereas the time constants were significantly larger for the other mutants ranging from 1060 to 1528 ns. Fitting parameters are given in Tables S6 and S7. Despite the fluctuations in the helicity, the model is able to differentiate between the different thermal unfolding rates.

Reduced Unfolding of Membrane-Inserted β-Tongue Y178F Mutant. The thermal unfolding simulations of the monomer illustrate the differential flexibility in key membrane-binding motifs between the WT and the mutants. Since the Y178F mutant is the only point mutation in the membrane-inserted β-tongue region, we carried out simulations of the β-tongue, Y178F motif in the membrane environment to see if we could draw a connect with the thermal unfolding simulations. The average of three independent replicates are analyzed and various properties are compared with the WT membrane-inserted protein as illustrated in Figure 6A. Analysis of the time evolution of both the RMSD (Figure 6B) and radius of gyration (R_g) (Figure 6C) clearly illustrate the increased rigidity of the Y178F mutant when compared with the WT. Lowered fluctuations are observed in the RMSFs as well (Figure 6D). Evolution of the secondary structure (Figure 6E) illustrates greater secondary structure changes being induced in the WT and an increased tendency toward coil formation. However, the secondary structure changes are significantly lowered in the case of the Y178F mutant indicating that the mutant shows a distinct resistance to unfolding when compared with the WT. These observations for the membrane-inserted simulations at 310 K correlate extremely well with the enhanced flexibility and increased secondary structure changes observed in the thermal unfolding simulations at 400 K for the WT when compared with the Y178F mutant. We attempted to study the free energy of transition to the helix-turn-helix motif as we had carried out for the WT; however, we were unable to sample the intermediate hinged state (Figure 2E) that was stabilized for the WT. While setting up the initial position of Y178F as hinged to the membrane, we also observed a tendency for the mutant to move toward the upper leaflet headgroups of the bilayer (Figure S1D). The Y residue is part of the RKWY set of residues that play an important role in anchoring membrane proteins to the lipid headgroups and Y178 has shown to play a similar role for the β-tongue.[20] Our simulations further reinforce this loss of hinging with the Y178F mutant. Given this situation, we did not attempt to compute the free energy of the transition as the Z-coordinate of the protein center of mass would also need to be included in the collective variable space. We will show later that the Y178F mutation results in a complete loss of lytic activity, indicating compromised pore formation, compromised binding, and/or compromised secondary structure changes in the membrane.

Membrane-Inserted Protomer ClyA Mutants Are Compromised Structurally with Defects in Membrane Insertion. We also examined the effect of mutations on the protomer pore state using 1 μs long MD simulations of a ClyA trimer in a POPC/cholesterol (70:30) lipid membrane. While the protomer state might not manifest readily in some of these mutants due to their compromised ability to undergo the structural transition, we speculated that mutations in ClyA would display destabilization in the pore-like state. Considering the central protomer in the trimer as representative of a protomer reflecting interactions in the full-pore and higher order oligomers, we evaluated its flexibility upon mutation. These simulations were all carried out at 310 K.

RMSD time trajectories of the ClyA trimer and the central protomer indicate that the membrane-inserted states have equilibrated beyond 400 ns (Figure S6, parts A and B). Hence, we utilize the next 600 ns of the simulation trajectory for subsequent analysis. Average RMSD of the β-tongue region for the β-tongue mutant (Y178F) is 1.5-fold larger than that of the WT protein (Figure 7A) suggesting increased structural

https://doi.org/10.1021/acs.jpcb.2c05785
J. Phys. Chem. B 2023, 127, 69−84

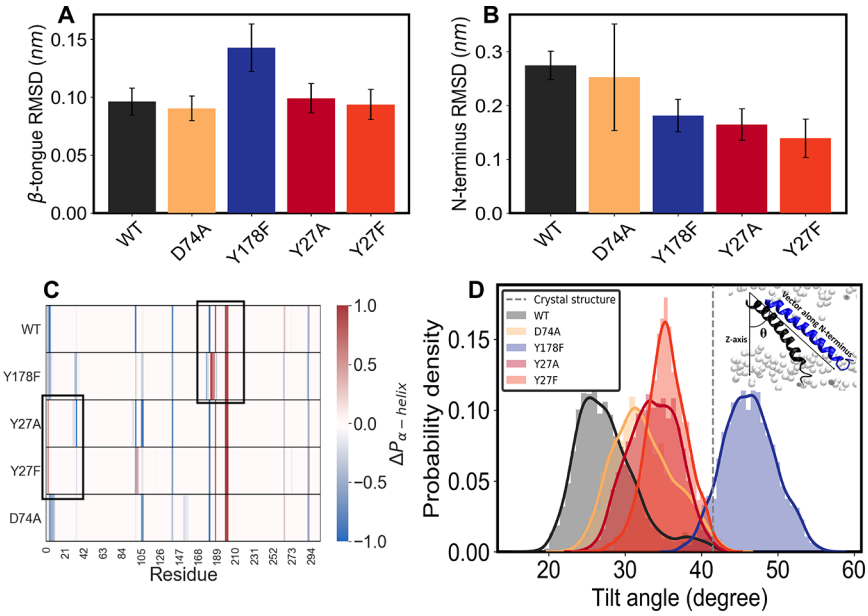

Figure 7. Protomer structural analysis from ClyA trimer-membrane simulations at 310 K. (A) RMSD comparison of the β-tongue region of the central protomer. (B) RMSD comparison of N-terminus helix of the central protomer. (C) ΔP_i (eq 6), calculated for the α-helical content change of the central protomer with respect to the crystal structure of the ClyA pore state. Positive values (red) indicates an increase in helicity and negative values (blue) indicate a decrease in helicity. Black boxes indicate the regions where an increase in helicity is observed. (D) Probability density distribution of tilt angle of the N-terminus helix for the central protomer. Inset: Tilt angles were calculated between a vector normal to the membrane and a vector from the first and last residue of the N-terminus as illustrated. Representative positions of the N-terminus helix for WT (black) and Y178F (blue) ClyA are depicted.

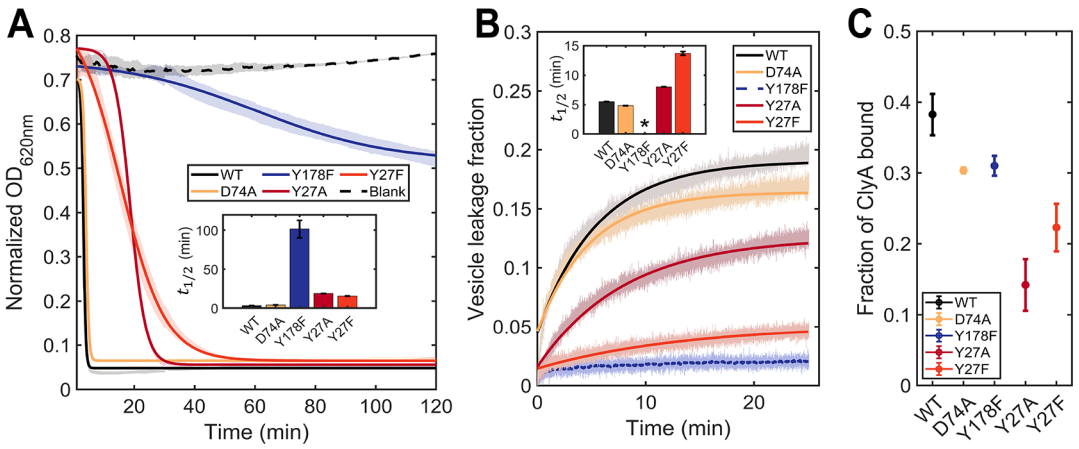

Figure 8. Lytic activity, vesicle leakage, and membrane binding by ClyA proteins. (A) Erythrocyte turbidity assay to determine the activity of ClyA mutants is performed by measuring the optical density (OP) of rabbit erythrocytes upon addition of the protein. Solid lines represent Boltzmann sigmoid fits (eq 7) to the data (see Table S4). $t_{1/2}$ is shown in the inset figure. (B) Vesicle dye leakage kinetics of ClyA mutants for 70% POPC and 30% cholesterol membranes. Solid lines represent single exponential fits (eq 8) to the leakage data (see Table S5). Dye leakage $t_{1/2}$ is shown in the inset figure. (C) Fraction of ClyA bound to red blood cells estimated from the loss of labeled ClyA from solution.

variation and flexibility in the region. While the Y27 residue points toward the pocket between adjacent β-tongue motifs, both mutations in Y27 did not alter the RMSD in the β-tongue region. On the other hand, a comparison of the RMSD of the N-terminus region (Figure 7B) suggests that the N-terminus structural deviation from the crystal structure has been reduced for all mutants except for the salt-bridge D74A mutant. Therefore, the β-tongue mutation compromises the flexibility of the β-tongue in the membrane while the N-terminus helix loses flexibility upon mutations.

We next probe the overall secondary structure changes in the protomer among the mutants by comparing the change in the α-helical content (eq 6) with respect to the crystal structure (Figure 7C) for the central protomer in the membrane-inserted trimer. The Y178F mutant showed an increase in α helicity in the turn region of the helix-turn-helix motif of the membrane-inserted β-tongue and a decrease in the 3_{10}-helicity (see Figure S8). The STRIDE analysis (see Figure S7) illustrates the time evolution of the changes in the β-tongue region of the mutant. Structures of the mutants at the end of the 1 μs of simulation are shown in Figure S9, where secondary structures of the membrane interacting motifs are highlighted. The increased helicity displayed by Y178F in the turn region suggests that the helix-turn-helix motif as observed in the crystal structure is not a favorable configuration. We further analyzed the N-terminus behavior by quantifying the

https://doi.org/10.1021/acs.jpcb.2c05785
J. Phys. Chem. B 2023, 127, 69−84

tilt angle of the N-terminus to determine the extent of membrane insertion of this motif. All the mutants (and especially Y178F) display a significantly larger tilt angle compared to the WT (Figure 7D) indicating that the propensity of the N-terminus to traverse the membrane is compromised.

Point Mutations in β-Tongue and N-Terminus Helix Curtail ClyA Lytic Activity. Next, we examined the effect of the point mutations on hemolytic activity, vesicle leakage, and the membrane binding of ClyA (Figure 8). Using erythrocyte turbidity assays (Figure 8A), we find that the disruption of a stable salt bridge between D74-K240/N142 residues by an Asp-Ala substitution at position 74 (D74A) did not perturb ClyA cell lysis activity significantly. On the other hand, β-tongue (Y178F) and N-terminal (Y27A and Y27F) mutants disrupt ClyA activity to different degrees. The β-tongue mutant displays a ≥30-fold increase in $t_{1/2}$ for cell lysis. The N-terminus mutants also display a marked but smaller reduction ($t_{1/2}$ increase by ∼3 fold) in lysis activity with Y27A displaying faster kinetics (but a delayed onset of lysis) when compared with Y27F. Vesicle leakage experiments (Figure 8B) demonstrate a similar activity trend for all the mutants, with D74A displaying WT-like activity; both Y27 (N-terminus) mutations lead to a ∼ 2−3 fold decrease in vesicle poration, and complete loss of function is evident in the Y178F mutant. This confirms that loss of cell lysis activity in these mutants arises from their inability to porate the lipid membrane. Binding of the N-terminus mutants to RBCs (Figure 8C) were lower (∼3 fold) as compared to β-tongue and salt bridge mutant, suggesting that the N-terminus also has a significant role in direct membrane binding[5,8] in addition to inducing the protomer state. Even though the N-terminus mutants (Y27A and Y27F) show less binding in comparison to the WT, both show delayed activity (Figure 8, parts A and B). Since the measurement of the binding is at equilibrium, the lower binding might be due to faster unbinding kinetics and slower binding kinetics.

Therefore, a key finding from comparison of the pore forming activity observed in experiments to thermal unfolding simulations of the ClyA mutants is the reduced flexibility in the β-tongue motif and the resistance to lose secondary structure correlates closely with diminished ClyA lytic activity. Combined with the free energy computations of the membrane-inserted β-tongue, which reveals the presence of an unfolded intermediate in the folding pathway, our study illustrates that the inherent flexibility in the β-tongue is a key driver for the membrane-induced transition to a helix-turn-helix motif and eventual pore formation.

DISCUSSION

A key step in the membrane-driven pore-forming mechanism of ClyA is the initial binding of the predominantly hydrophobic β-tongue residues with the membrane. In order for this interaction to occur, the hydrophobic β-tongue motif, which is buried within the four helix bundle of the ClyA monomer, must swing outward to bind with the membrane.[3,23,41] Although there is no direct experimental evidence for this proposed pathway, several mutational studies in the β-tongue region point to the central role played by this motif,[7,24,42,43] and structure-based MD simulations reveal this as the dominant pathway.[3,5] However, molecular details of the subsequent secondary structure transitions that occur during ensuing oligomerization are unknown.

Our all-atom MD simulations and string method based free energy computation of the transition in the membrane provide for the first time, direct evidence for the unfolding of the β-tongue in the monomer as an initial step in the conformational transition. This tendency for the β-tongue to unfold is observed in simulations of both the full monomer as well as the membrane-inserted β-tongue motif. Combined with the string method computations, we identify this partially unfolded state as an on-pathway intermediate during ClyA pore formation. A β-tongue mutant motif (Y178F) which shows lowered flexibility resists membrane-assisted unfolding correlating with reduced lytic activity for this mutant. These simulations combined with the lysis and leakage experiments indicate that the loss of structural flexibility correlates positively with mitigating pore forming activity.

With the inherent challenges associated with obtaining free energy landscapes for the complete transition from water-soluble monomer to the membrane-inserted state, we carried out extensive replicate thermal unfolding molecular dynamics simulations at 400 K of the ClyA monomer and its mutants to understand the influence of point mutations in critical regions implicated in membrane binding and the conformational transitions. With the exception of D74A which showed similar behavior as the WT and served as a positive control in both experiments and simulations, all other mutants showed a pronounced loss of flexibility as revealed in the RMSF data at 400 K across the entire protein. The changes in both the RMSF and RMSD were distinctly higher in the β-tongue region of the WT protein, indicating that mutations resulted in greater resistance to structural changes. Tracking the flexibility of the β-tongue hinge location in the monomer gave us several interesting cues to the conformational transition hurdle induced by the mutations in this study. Virtual springs modeled as harmonic oscillators between critical residues associated with the movement around the hinge regions (G180 and G201) of β-tongue quantified the increased stiffness observed in all mutants when compared with the WT and D74A mutant. While the present analysis is based on structural metrics, a more detailed molecular analysis would be needed to decipher the molecular interactions responsible for the observed loss in flexibility due to the mutations.

Correlating with the propensity to disorder, erythrocyte rupture and vesicle leakage experiments which provide direct evidence of pore formation, reveal a near complete loss of activity for the β-tongue mutant, Y178F and compromised or delayed activity for the N-terminal mutants, Y27A and Y27F, with little change in the activity for the D74A mutant. Thus, experiments further reinforce the findings from the MD simulations supporting the view that a tendency to lose secondary structure is essential for pore formation. The reduced lytic activity for the Y178F mutants is consistent with the loss of flexibility observed in the simulations.

Furthermore, our membrane-inserted trimeric arc simulations reinforced the effect of the loss of flexibility on a proper conformational change, where we observed a tendency for destabilization of the β-tongue for Y178F. The translocation of N-terminus across the membrane was also found to be affected due to point mutations, with Y178F showing greater tendency for pore closure correlating with its high loss of activity. We alert the reader that simulations of pore states or partially formed pore states with the Y178F mutant that did not show lytic activity in the experiments should be interpreted with some caution since preassembled pore states deduced from the

https://doi.org/10.1021/acs.jpcb.2c05785
J. Phys. Chem. B 2023, 127, 69−84

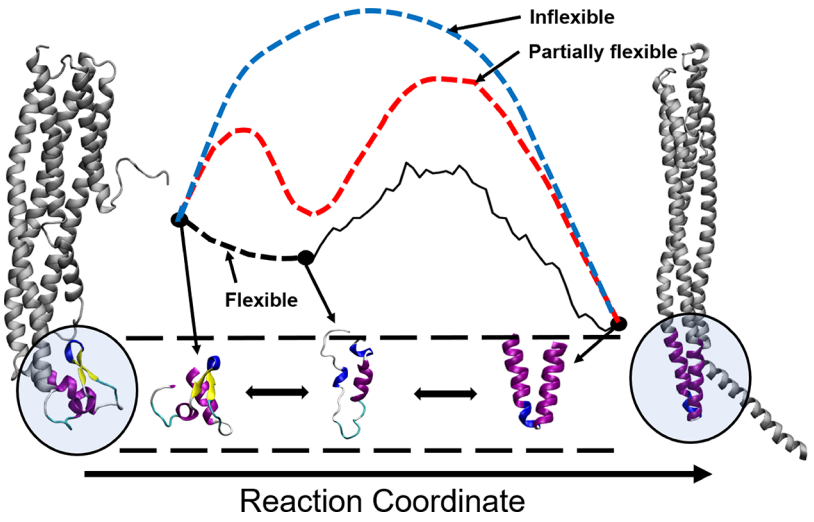

Figure 9. Proposed changes in the free energy landscape upon mutation. The free energy profiles for the β-tongue to transition to an unfolded intermediate and refold to the helix-turn-helix motif are illustrated for the different mutants. The black line is the computed free energy profile from an unfolded state to the protomer state of WT with the initial spontaneous unfolding represented as a dashed line. Since the D74A mutant has similar activity as the WT, we propose that this mutant follows a similar free energy profile illustrated by the black line. Dashed lines are hypothetical free energy profiles for the N-terminal mutants (red) where lytic activity is delayed and the Y178F mutant (blue) where kinetics is significantly lowered.

crystal structure of the WT protein might not realistically represent the structures of the mutants.

A common theme that emerges in our study is the correlation between the observed increased lytic ability and the enhanced disorder or "plasticity" associated with the monomer. This specific feature, wherein conformational transitions are assisted by the presence of a disordered state is gaining acceptance and extensively investigated in intrinsically disordered proteins (IDPs).[44−50] The inherent flexibility in IDPs play a central role in allowing them to transition from a disordered to ordered state upon binding to a target molecule.[51−53] Our findings suggest that the pre-existing functional disorder in IDPs is more universal and appears to be exploited by the bistable ClyA protein for optimal functionality during the conformational transition and subsequent oligomerization that occurs from the water-soluble monomeric state to the membrane-inserted protomer. We report for the first time that a finely tuned conformational flexibility is essential for the activity of a pore-forming toxin (ClyA). The inherent flexibility of the β-tongue region of the ClyA, which undergoes a large conformational change from a β-sheet to a helix-turn helix motif, was found to be the crucial. We hypothesize that this flexibility is essential for the membrane-mediated conformational change, assembly and pore formation of ClyA. Interestingly, simulations of the monomer with the β-tongue embedded in the membrane were also seen to influence the behavior of the N-terminus (Figure 2C), where both these membrane motifs start to unfold. This suggests that the β-tongue and the N-terminus have a strong allosteric effect, and the unfolding of the β-tongue is correlated with the motion of the N-terminus during pore formation. This connection could arise from the hydrophobic interaction between the tip residue (F190) of β-tongue and the end residue (F50) of N-terminus (Figure 4) as suggested by Mueller et al.[3] Although our study provides several molecular insights into ClyA pore formation, the precise sequence of steps and whether unfolding in the N-terminus is a precursor to membrane insertion is unexplored. Interestingly, the N-terminal mutants also resulted in increased rigidity in the β-tongue residues illustrating the presence of allosteric effects between these two motifs. Both the N-terminal mutants investigated in this study show delayed lytic ability in contrast to the β-tongue mutant where activity is significantly reduced. Our study further shows that mutations that compromise this inherent tendency to prevent disorder in critical membrane-binding motifs and lose secondary structure can drastically limit and abrogate the pore forming pathway and subsequent lytic ability of ClyA. Indeed, recent single molecule FRET experiments[39] to examine the unfolding pathway of ClyA reveal the presence of partially folded intermediates with unfolded C- and N-termini, and earlier ensemble experiments in detergent point to the formation of a molten globule intermediate during the pore assembly pathway.[38]

We summarize our combined findings from the simulations and experiments in terms of the proposed free energy landscapes (dashed lines) for the different mutants as illustrated in Figure 9. The free energy landscape for the WT and D74A depict inherent protein flexibility, spontaneously converting into the on-pathway unfolded intermediate prior to forming the folded protomer motif whose free energy barrier was computed using the string method. However, the N-terminal mutants (Y27A, Y27F) showed a delayed activity in the experiments, suggesting the presence of a barrier (red dashed line, Figure 9) for unfolding and subsequent refolding. In the case of Y178F, where pore forming activity and kinetics are significantly reduced, the associated free energy landscape is depicted with the largest barrier (blue dashed line) for membrane-associated secondary structure changes.

The dynamics of the mutants and the WT can further be studied by varieties of techniques. The first is related to the experimental lysis and leakage data and we have previously modeled leakage kinetics using rate based approaches[54,55] to delineate specific oligomerization pathways during pore formation. It is possible to apply these kinetic models for the mutants and wild type proteins to decipher the pathways and lowered kinetics observed for the mutants. However, we did

https://doi.org/10.1021/acs.jpcb.2c05785
J. Phys. Chem. B 2023, 127, 69−84

not pursue this approach in this manuscript. The second aspect of dynamics is related to the thermal unfolding. In order to differentiate between the kinetics of unfolding, we used a simple first order kinetic model to compare and differentiate between the thermal unfolding rates (Figure 5, parts C and D). While extracting dynamic variables such as spring constants one must note that the thermal unfolding trajectories are represent nonequilibrium situations and extracting and interpreting dynamic variables must be carried out with caution. We however only use these constants to differentiate between the different mutants. Finally, one could also obtain rates from the free energy landscape using mean first passage time based approaches.[56] These methods are computationally challenging for membrane-inserted proteins with the higher dimensional collective variable space used in this work.

Before concluding, we point out that despite the inherently nonequilibrium nature of the thermal unfolding simulations at 400 K, we were able to extract differences in the unfolding tendencies between the mutants thereby serving as a reliable proxy for membrane-induced secondary structure changes. Additionally, the enhanced unfolding, largely localized to the β-tongue region in the thermal unfolding simulations was qualitatively similar to the unfolding observed in the membrane at room temperature for the WT.

In reality, the conformational change of the monomer to protomer would include partial unfolding and refolding events in the proximity or inside the membrane. Although the protein might progressively denature at 400 K at a longer time scale (several tens of microseconds to seconds) it is the initial unfolding of the essential motifs that provides crucial information for the conformational changes at room temperature as suggested by the monomer inserted in the membrane simulations. In our work, we assess this initial unfolding of the monomer and its mutants to study the link between protein flexibility and the resulting unfolding and finally correlate with pore formation as observed in the lytic activity in the experiments with vesicles and erythrocytes.

CONCLUSION

Our study illustrates that for the inherent flexibility in the α-PFT, ClyA is essential for a robust conformational transition to the membrane-inserted protomeric state. Our combined free energy and thermal unfolding simulations illustrate that flexibility in the membrane interacting motifs of the monomer state allows a loss of secondary structure, to enable sampling an on-pathway unfolded intermediate. Thermal unfolding molecular dynamics simulations of monomer and its point mutants reveal a direct link between the loss of flexibility in key membrane interrogating motifs with reduced lytic ability as revealed in both erythrocyte lysis and vesicle leakage experiments with ClyA.

Our study not only reinforces the view that the β-tongue is a central driver in the pore-forming pathway of ClyA but also illustrates that the structural flexibility of essential motifs that interact with the membrane are a key to their functionality. The notion that protein flexibility or tendency to disorder is essential for structural transformations is similar to the folding phenomenon observed in IDPs. Although relatively unexplored in connection with the pore forming pathways for PFTs, our study suggests that inherent disorder could be a more general phenomenon prevalent across a wider class of PFTs that form large membrane-inserted oligomeric assemblies. These findings can potentially help in the development of novel drug targets to combat PFT-mediated bacterial infections to either inhibit or retard the kinetics of pore formation.

ASSOCIATED CONTENT

Supporting Information

The Supporting Information is available free of charge at https://pubs.acs.org/doi/10.1021/acs.jpcb.2c05785.

Figures showing truncated β-tongue in the membrane, ClyA monomer Ramachandran map, ClyA monomer simulation analysis, ClyA monomer secondary structure analysis, residue-wise secondary structure analysis of ClyA monomer, protomer simulation analysis in membrane-embedded trimeric arc, membrane-inserted trimer arc secondary structure analysis of central protomer, residue-wise secondary structure analysis of membrane-inserted trimer arc, and central protomer, membrane-inserted trimer arc representation and tables of ClyA monomer simulation details, membrane-inserted trimer arc simulation details, membrane-inserted monomer simulation details, fitting parameters of Boltzmann sigmoidal function of RBC turbidity assay experiments. fitting parameters of exponential curve of vesicle leakage experiments, and fitting parameters of exponential curves (PDF)

AUTHOR INFORMATION

Corresponding Authors

Rahul Roy − *Department of Chemical Engineering, Indian Institute of Science, Bangalore, Karnataka 560012, India; Center for BioSystems Science and Engineering, Indian Institute of Science, Bangalore, Karnataka 560012, India;* orcid.org/0000-0003-3329-8803; Email: rahulroy@iisc.ac.in

K. Ganapathy Ayappa − *Department of Chemical Engineering, Indian Institute of Science, Bangalore, Karnataka 560012, India;* orcid.org/0000-0001-7599-794X; Email: ayappa@iisc.ac.in

Authors

Avijeet Kulshrestha − *Department of Chemical Engineering, Indian Institute of Science, Bangalore, Karnataka 560012, India*

Satyaghosh Maurya − *Department of Chemical Engineering, Indian Institute of Science, Bangalore, Karnataka 560012, India*

Twinkle Gupta − *Department of Chemical Engineering, Indian Institute of Science, Bangalore, Karnataka 560012, India*

Sudeep N Punnathanam − *Department of Chemical Engineering, Indian Institute of Science, Bangalore, Karnataka 560012, India;* orcid.org/0000-0002-3703-9158

Complete contact information is available at: https://pubs.acs.org/10.1021/acs.jpcb.2c05785

Notes

The authors declare no competing financial interest.

ACKNOWLEDGMENTS

We would like to thank Benjamin Schuler from the University of Zurich for sharing the pET11a-ClyAQ56C plasmid, Sunaina Banerjee from IISc for assisting with the mutations, and

Ramesh Cheerla for providing the initial configurations for the membrane-inserted trimeric arc simulations. We acknowledge the Supercomputer Education and Research Center (SERC) computing facility, Thematic Unit of Excellence on Computational Materials Science (TUE-CMS), a Department of Science and Technology (DST) supported computing facility at the Indian Institute of Science Bangalore and the National Supercomputing Mission, India, for funding used in this work.

REFERENCES

(1) Bischofberger, M.; Iacovache, I.; Van Der Goot, F. G. Pathogenic pore-forming proteins: function and host response. *Cell Host & Microbe* **2012**, *12*, 266−275.
(2) Dal Peraro, M.; Van Der Goot, F. G. Pore-forming toxins: ancient, but never really out of fashion. *Nature Reviews Microbiology* **2016**, *14*, 77−92.
(3) Mueller, M.; Grauschopf, U.; Maier, T.; Glockshuber, R.; Ban, N. The structure of a cytolytic α-helical toxin pore reveals its assembly mechanism. *Nature* **2009**, *459*, 726−730.
(4) Oscarsson, J.; Mizunoe, Y.; Li, L.; Lai, X.-H.; Wieslander, Å.; Uhlin, B. E. Molecular analysis of the cytolytic protein ClyA (SheA) from Escherichia coli. *Mol. Microbiol.* **1999**, *32*, 1226−1238.
(5) Giri Rao, V. H.; Desikan, R.; Ayappa, K. G.; Gosavi, S. Capturing the membrane-triggered conformational transition of an α-helical pore-forming toxin. *J. Phys. Chem. B* **2016**, *120*, 12064−12078.
(6) Behera, A.; Ayappa, K. G. Molecular dynamics simulations Reveal the Role of Membrane Cholesterol during Pore Forming Pathway of Cytolysin A. M.Sc. Thesis, Indian Institute of Science: Bangalore, India, 2018.
(7) Ludwig, A.; Völkerink, G.; von Rhein, C.; Bauer, S.; Maier, E.; Bergmann, B.; Goebel, W.; Benz, R. Mutations affecting export and activity of cytolysin A from Escherichia coli. *J. Bacteriol.* **2010**, *192*, 4001−4011.
(8) Sathyanarayana, P.; Maurya, S.; Behera, A.; Ravichandran, M.; Visweswariah, S. S.; Ayappa, K. G.; Roy, R. Cholesterol promotes cytolysin A activity by stabilizing the intermediates during pore formation. *Proc. Natl. Acad. Sci. U. S. A.* **2018**, *115*, E7323−E7330.
(9) Branduardi, D.; Gervasio, F. L.; Parrinello, M. From A to B in free energy space. *J. Chem. Phys.* **2007**, *126*, 054103.
(10) Kulshrestha, A.; Punnathanam, S.; Ayappa, G. Finite temperature string method with umbrella sampling using path collective variables: Application to secondary structure change in a protein. *Soft Matter* **2022**, *18*, 7593−7603.
(11) E, W.; Ren, W.; Vanden-Eijnden, E. Finite temperature string method for the study of rare events. *J. Phys. Chem. B* **2005**, *109*, 6688−6693.
(12) Song, H. D.; Zhu, F. Finite Temperature String Method with Umbrella Sampling: Application on a Side Chain Flipping in Mhp1 Transporter. *J. Phys. Chem. B* **2017**, *121*, 3376−3386.
(13) Pan, A. C.; Sezer, D.; Roux, B. Finding transition pathways using the string method with swarms of trajectories. *J. Phys. Chem. B* **2008**, *112*, 3432−3440.
(14) Caflisch, A.; Karplus, M. *The protein folding problem and tertiary structure prediction*; Springer: 1994; pp 193−230.
(15) Huet, A.; Derreumaux, P. Impact of the mutation A21G (Flemish variant) on Alzheimer's β-amyloid dimers by molecular dynamics simulations. *Biophys. J.* **2006**, *91*, 3829−3840.
(16) Walser, R.; Mark, A. E.; Van Gunsteren, W. F. On the temperature and pressure dependence of a range of properties of a type of water model commonly used in high-temperature protein unfolding simulations. *Biophys. J.* **2000**, *78*, 2752−2760.
(17) Dinner, A. R.; Karplus, M. Is protein unfolding the reverse of protein folding? A lattice simulation analysis. *J. Mol. Biol.* **1999**, *292*, 403−419.
(18) Klimov, D. K.; Thirumalai, D. Symmetric connectivity of secondary structure elements enhances the diversity of folding pathways. *J. Mol. Biol.* **2005**, *353*, 1171−1186.
(19) Creighton, T. E. Toward a better understanding of protein folding pathways. *Proc. Natl. Acad. Sci. U. S. A.* **1988**, *85*, 5082−5086.
(20) Varadarajan, V.; Desikan, R.; Ayappa, K. G. Assessing the extent of the structural and dynamic modulation of membrane lipids due to pore forming toxins: insights from molecular dynamics simulations. *Soft Matter* **2020**, *16*, 4840−4857.
(21) Fantini, J.; Barrantes, F. J. How cholesterol interacts with membrane proteins: an exploration of cholesterol-binding sites including CRAC, CARC, and tilted domains. *Frontiers in Physiology* **2013**, *4*, 31.
(22) Desikan, R.; Maiti, P. K.; Ayappa, K. G. Predicting interfacial hot-spot residues that stabilize protein-protein interfaces in oligomeric membrane-toxin pores through hydrogen bonds and salt bridges. *J. Biomol. Struct. Dyn.* **2021**, *39*, 20−34.
(23) Desikan, R.; Maiti, P. K.; Ayappa, K. G. Assessing the structure and stability of transmembrane oligomeric intermediates of an α-helical toxin. *Langmuir* **2017**, *33*, 11496−11510.
(24) Wallace, A. J.; Stillman, T. J.; Atkins, A.; Jamieson, S. J.; Bullough, P. A.; Green, J.; Artymiuk, P. J. E. coli hemolysin E (HlyE, ClyA, SheA): X-ray crystal structure of the toxin and observation of membrane pores by electron microscopy. *Cell* **2000**, *100*, 265−276.
(25) Humphrey, W.; Dalke, A.; Schulten, K. VMD: visual molecular dynamics. *J. Mol. Graphics* **1996**, *14*, 33−38.
(26) Huang, J.; MacKerell, A. D., Jr CHARMM36 all-atom additive protein force field: Validation based on comparison to NMR data. *J. Comput. Chem.* **2013**, *34*, 2135−2145.
(27) Dingfelder, F.; Macocco, I.; Benke, S.; Nettels, D.; Faccioli, P.; Schuler, B. Slow Escape from a Helical Misfolded State of the Pore-Forming Toxin Cytolysin A. *JACS Au* **2021**, *1*, 1217−1230.
(28) Jo, S.; Kim, T.; Iyer, V. G.; Im, W. CHARMM-GUI: a web-based graphical user interface for CHARMM. *J. Comput. Chem.* **2008**, *29*, 1859−1865.
(29) Fiser, A.; Do, R. K. G.; et al. Modeling of loops in protein structures. *Protein Sci.* **2000**, *9*, 1753−1773.
(30) Pronk, S.; Páll, S.; Schulz, R.; Larsson, P.; Bjelkmar, P.; Apostolov, R.; Shirts, M. R.; Smith, J. C.; Kasson, P. M.; van der Spoel, D.; et al. GROMACS 4.5: a high-throughput and highly parallel open source molecular simulation toolkit. *Bioinformatics* **2013**, *29*, 845−854.
(31) Wang, J.; Wolf, R. M.; Caldwell, J. W.; Kollman, P. A.; Case, D. A. Development and testing of a general Amber force field. *J. Comput. Chem.* **2004**, *25*, 1157−1174.
(32) Jambeck, J. P.; Lyubartsev, A. P. Derivation and systematic validation of a refined all-atom force field for phosphatidylcholine lipids. *J. Phys. Chem. B* **2012**, *116*, 3164−3179.
(33) Ponmalar, I. I.; Cheerla, R.; Ayappa, K. G.; Basu, J. K. Correlated protein conformational states and membrane dynamics during attack by pore-forming toxins. *Proc. Natl. Acad. Sci. U. S. A.* **2019**, *116*, 12839−12844.
(34) Desikan, R.; Padmanabhan, P.; Ayappa, K. G. Opening of smaller toxin pores by lipid micelle formation. *Proc. Natl. Acad. Sci. U. S. A.* **2020**, *117*, 5107−5108.
(35) Allouche, A.-R. Gabedit—A graphical user interface for computational chemistry softwares. *J. Comput. Chem.* **2011**, *32*, 174−182.
(36) Kabsch, W.; Sander, C. Dictionary of protein secondary structure: pattern recognition of hydrogen-bonded and geometrical features. *Biopolymers: Original Research on Biomolecules* **1983**, *22*, 2577−2637.
(37) Frishman, D.; Argos, P. Knowledge-based protein secondary structure assignment. *Proteins: Struct., Funct., Bioinf.* **1995**, *23*, 566−579.
(38) Benke, S.; Roderer, D.; Wunderlich, B.; Nettels, D.; Glockshuber, R.; Schuler, B. The assembly dynamics of the cytolytic pore toxin ClyA. *Nat. Commun.* **2015**, *6*, 1−15.
(39) Dingfelder, F.; Benke, S.; Nettels, D.; Schuler, B. Mapping an equilibrium folding intermediate of the cytolytic pore toxin ClyA with single-molecule FRET. *J. Phys. Chem. B* **2018**, *122*, 11251−11261.

https://doi.org/10.1021/acs.jpcb.2c05785
J. Phys. Chem. B 2023, 127, 69−84

(40) Atkins, A.; Wyborn, N. R.; Wallace, A. J.; Stillman, T. J.; Black, L. K.; Fielding, A. B.; Hisakado, M.; Artymiuk, P. J.; Green, J. Structure-function relationships of a novel bacterial toxin, hemolysin E: the role of αG. *J. Biol. Chem.* **2000**, *275*, 41150−41155.
(41) Sathyanarayana, P.; Visweswariah, S. S.; Ayappa, K. G. Mechanistic insights into pore Formation by an α-Pore forming toxin: Protein and lipid bilayer interactions of cytolysin A. *Acc. Chem. Res.* **2021**, *54*, 120−131.
(42) Wai, S. N.; Westermark, M.; Oscarsson, J.; Jass, J.; Maier, E.; Benz, R.; Uhlin, B. E. Characterization of dominantly negative mutant ClyA cytotoxin proteins in Escherichia coli. *J. Bacteriol.* **2003**, *185*, 5491−5499.
(43) Wyborn, N. R.; Clark, A.; Roberts, R. E.; Jamieson, S. J.; Tzokov, S.; Bullough, P. A.; Stillman, T. J.; Artymiuk, P. J.; Galen, J. E.; Zhao, L.; et al. Properties of haemolysin E (HlyE) from a pathogenic Escherichia coli avian isolate and studies of HlyE export. *Microbiology* **2004**, *150*, 1495−1505.
(44) Shirai, N. C.; Kikuchi, M. Structural flexibility of intrinsically disordered proteins induces stepwise target recognition. *J. Chem. Phys.* **2013**, *139*, 225103.
(45) Bhattarai, A.; Emerson, I. A. Dynamic conformational flexibility and molecular interactions of intrinsically disordered proteins. *Journal of Biosciences* **2020**, *45*, 1−17.
(46) Borgia, A.; Borgia, M. B.; Bugge, K.; Kissling, V. M.; Heidarsson, P. O.; Fernandes, C. B.; Sottini, A.; Soranno, A.; Buholzer, K. J.; Nettels, D.; et al. Extreme disorder in an ultrahigh-affinity protein complex. *Nature* **2018**, *555*, 61−66.
(47) Tompa, P.; Fuxreiter, M. Fuzzy complexes: polymorphism and structural disorder in protein-protein interactions. *Trends Biochem. Sci.* **2008**, *33*, 2−8.
(48) Arbesú, M.; Iruela, G.; Fuentes, H.; Teixeira, J.; Pons, M. Intramolecular fuzzy interactions involving intrinsically disordered domains. *Frontiers in Molecular Biosciences* **2018**, *5*, 39.
(49) Uversky, V. N.; Dunker, A. K. Multiparametric analysis of intrinsically disordered proteins: looking at intrinsic disorder through compound eyes. *Anal. Chem.* **2012**, *84*, 2096−2104.
(50) Abrams, C.; Bussi, G. Enhanced sampling in molecular dynamics using metadynamics, replica-exchange, and temperature-acceleration. *Entropy* **2014**, *16*, 163−199.
(51) Troilo, F.; Bonetti, D.; Bignon, C.; Longhi, S.; Gianni, S. Understanding intramolecular crosstalk in an intrinsically disordered protein. *ACS Chem. Biol.* **2019**, *14*, 337−341.
(52) Kjaer, L.; Giehm, L.; Heimburg, T.; Otzen, D. The influence of vesicle size and composition on α-synuclein structure and stability. *Biophys. J.* **2009**, *96*, 2857−2870.
(53) Jain, N.; Bhasne, K.; Hemaswasthi, M.; Mukhopadhyay, S. Structural and dynamical insights into the membrane-bound α-synuclein. *PloS one* **2013**, *8*, e83752.
(54) Agrawal, A.; Apoorva, K.; Ayappa, K. Transmembrane oligomeric intermediates of pore forming toxin Cytolysin A determine leakage kinetics. *RSC Adv.* **2017**, *7*, 51750−51762.
(55) Vaidyanathan, M.; Sathyanarayana, P.; Maiti, P. K.; Visweswariah, S. S.; Ayappa, K. Lysis dynamics and membrane oligomerization pathways for Cytolysin A (ClyA) pore-forming toxin. *RSC Adv.* **2014**, *4*, 4930−4942.
(56) Wedekind, J.; Strey, R.; Reguera, D. New method to analyze simulations of activated processes. *J. Chem. Phys.* **2007**, *126*, 134103.

https://doi.org/10.1021/acs.jpcb.2c05785
J. Phys. Chem. B 2023, 127, 69−84